Available online at www.sciencedirect.com
ScienceDirect
Journal of Catalysis 251 (2007) 7–20
JOURNAL OF CATALYSIS
www.elsevier.com/locate/jcat

Combined steam reforming of methanol over Cu–Mn spinel oxide catalysts

Joan Papavasiliou [a,b], George Avgouropoulos [a], Theophilos Ioannides [a,*]

[a] *Foundation for Research and Technology-Hellas (FORTH), Institute of Chemical Engineering and High-Temperature Chemical Processes (ICE-HT), P.O. Box 1414, GR-26504 Patras, Greece*

[b] *Department of Chemical Engineering, University of Patras, GR-26500 Patras, Greece*

Received 2 May 2007; revised 20 July 2007; accepted 20 July 2007

Abstract

Cu–Mn spinel oxide catalysts were synthesized by the combustion method, and their behavior in the combined steam reforming of methanol was examined. It was found that despite their low surface areas, these catalysts had comparable activity to that of a commercial Cu–Zn–Al catalyst for the production of H_2 via (combined) steam reforming of methanol. The fresh Cu–Mn catalysts were composed of the spinel phase $Cu_{1.5}Mn_{1.5}O_4$, as well as Mn_2O_3 and CuO, depending on the Cu/Mn ratio, and were reduced to Cu^0 and MnO under reaction conditions. XPS analysis revealed the presence of two different oxidation states in both copper (Cu^{2+} and Cu^{+}) and manganese (Mn^{4+} and Mn^{3+}) in fresh catalysts and decomposition of the spinel in used catalysts. The optimal catalyst was prepared with a Cu/(Cu + Mn) ratio of 0.30. At a higher copper content ($x = 0.40, 0.50$), the excess copper was not incorporated into the spinel but instead was present as a separate CuO phase. A transient reduction/oxidation behavior was noted in the course of successive TPR/TPO cycles, as the efficiency of spinel reformation during oxidation of the reduced catalyst gradually diminished. The amount of CO produced from reforming was well below water–gas shift equilibrium, indicating that CO_2 was the primary product, whereas CO was produced by the reverse water–gas shift reaction. TPO measurements after methanol-reforming runs indicated only minimal carbon deposition.

Keywords: Hydrogen; Methanol; Combined steam reforming; Spinel; Copper oxide; Manganese oxide; Combustion method

1. Introduction

The increasing demand for energy (especially in developing nations), the uncertainty in energy prices, and the environmental impact of the conversion of fuels to energy, are 3 factors sparking the development of energy-conversion processes, such as fuel cells, that are efficient and have minimal environmental impact [1]. Fuel cells are appropriate for automotive applications, and their impact can be significant considering the current level of greenhouse gas emissions from automobiles [2]. Hydrogen is a clean fuel that can be produced from hydrocarbon reforming. Methanol is a leading candidate as hydrogen carrier, due to its high energy density, low sulfur content, easy availability, safe handling/storage, relatively low reforming temperatures, and low CO formation. Moreover, methanol may be derived from renewable energy sources. In such a case, a full environmental benefit is achieved, because no CO_2 emissions are added to the atmosphere, and fossil energy resources are preserved.

Hydrogen can be extracted from methanol via three process alternatives: thermal decomposition of methanol [Eq. (1)], partial oxidation of methanol [POM; Eq. (2)], and steam reforming of methanol [SRM; Eq. (3)] [2–4]:

$$CH_3OH \rightleftharpoons CO + 2H_2, \quad \Delta H^\circ = 92\ \text{kJ mol}^{-1}, \tag{1}$$

$$2CH_3OH + O_2 \rightarrow 2CO_2 + 4H_2, \quad \Delta H^\circ = -192.2\ \text{kJ mol}^{-1}, \tag{2}$$

$$CH_3OH + H_2O \rightleftharpoons CO_2 + 3H_2, \quad \Delta H^\circ = 49.4\ \text{kJ mol}^{-1}. \tag{3}$$

Thermal decomposition of methanol is an endothermic reaction that occurs at higher temperatures (up to 400 °C) than the other two processes. Moreover, it produces CO instead of CO_2 and thus is not applicable in PEM fuel cells, where CO poisons the Pt electrodes. POM is the only exothermic pathway for deriv-

* Corresponding author. Fax: +30 2610965223.
E-mail address: theo@iceht.forth.gr (T. Ioannides).

0021-9517/$ – see front matter
doi:10.1016/j.jcat.2007.07.025

ing hydrogen from methanol. The process occurs at moderate temperatures (200–220 °C) but it produces a lower H_2:CO_2 ratio (2:1) than SRM (3:1). Another significant drawback of POM is the formation of hot spots in the reactor. SRM is more suitable for fuel cell applications, because it occurs at moderate temperatures (200–300 °C) and produces more H_2 per mol of methanol. Its main drawbacks are the endothermicity of the reaction and the slow response at startup. An alternative approach is to combine POM and SRM by co-feeding oxygen, steam, and methanol to the reformer. The overall reaction is referred to as combined steam reforming of methanol (CSRM), or oxidative methanol reforming (OMR):

$$CH_3OH + (1-2\alpha)H_2O + \alpha O_2 \rightarrow CO_2 + (3-2\alpha)H_2 \quad (0 \leqslant \alpha \leqslant 0.5). \tag{4}$$

The reaction coefficient α can be adjusted in such a way so that the overall reaction is either thermally neutral or modestly exothermic, because the heat needed for the endothermic SRM is supplied by the exothermic POM reaction. Assuming prevaporized reactants, Eq. (4) is thermally neutral ($\Delta H^\circ = 0$ kJ mol^{-1}) when the oxygen-to-methanol ratio is equal to 0.1 [5]. Experimental studies on the CSRM process are limited compared with those concerning SRM and focus mainly on copper-based catalysts supported on ZnO, ZnO/Al_2O_3, or CeO_2 and group 8–10 metal-based catalysts supported on ZnO or ZnO/CeO_2 [6,7]. Huang and coworkers [8,9] determined the kinetics of CSRM over Cu–Zn–Al catalysts and proposed calculating the rate of the overall process by the sum of the rates of POM and SRM reactions. Velu et al. [10–12] investigated the effect of promoting Cu–Z–Al catalysts with Zr and Ce. Cu–Zn-based catalysts containing Zr exhibited higher catalytic activity in the CSRM reaction, which was attributed to the ease of reducibility and enhanced dispersion of copper particles. The substitution of Ce in the Cu–Zn–Al system did not significantly affect the catalytic performance. Agrell et al. [13] also studied the CSRM reaction over Cu/ZnO-based catalysts and found that Zr-containing catalysts performed well at high methanol conversions, but the Cu/ZnO catalyst was more efficient at low conversions; however, ZrO_2 suppressed CO formation. On the other hand, studies over an industrial copper-zinc oxide catalyst showed that it was deactivated with time on stream due to the agglomeration of copper [14]. We have proposed CuO–CeO_2 catalysts prepared by a urea combustion method [15,16]; we found these catalysts to be active for CSRM, with 99.7% methanol conversion obtained at 320 °C with 95% H_2 selectivity [15]. Similar catalytic behavior also was reported by Shan et al. [17].

We recently examined copper-manganese spinel oxide catalysts prepared following the urea–nitrate combustion method for the SRM process [18] and found these catalysts to be superior to CuO–CeO_2 catalysts prepared with the same technique, despite their low surface area. Their high activity was attributed to the formation of the spinel $Cu_xMn_{3-x}O_4$ phase in the fresh-oxidized catalysts. Optimal performance was achieved with the samples prepared with 75% excess of urea. In the present work, the catalytic performance of a series of Cu–Mn catalysts has been investigated for the CSRM process. The physicochemical properties of these catalysts both before and after exposure to the reaction mixture have been studied to gain insight into the origin of their high activity. The sample with the best catalytic performance was compared with a $Cu/ZnO/Al_2O_3$ commercial catalyst.

2. Experimental

2.1. Catalyst preparation

A series of copper–manganese oxide catalysts with Cu/(Cu + Mn) atomic ratios of 0 (Mn_2O_3), 0.10, 0.20, 0.30, 0.40, 0.50, and 1 (CuO) were prepared by the urea–nitrate combustion method as described previously [19]. A mixed solution of urea with manganese nitrate and copper nitrate with urea/nitrate molar ratio of 2.93 (75% excess of urea [19]) was autoignited in an open muffle furnace (preheated at 400–500 °C). To obtain pure, well-crystallized Cu–Mn catalysts, the powders were further heated at 550 °C for 1 h. All of the powders thus produced were sieved to obtain the desired fraction ($90 < d_p < 180$ μm). For ease of reference, the catalysts are designated Cu_xMn_{1-x}, where x is the Cu/(Cu + Mn) atomic ratio.

2.2. Catalyst characterization

Powder X-ray diffraction (XRD) patterns of the oxides were recorded with a Philips PW1830/40 powder diffractometer using nickel-filtered CuK_α radiation. The measurement was carried out in the 2θ angle range of 25°–85°. The specific surface area (S_{BET}) of the samples was measured by N_2 adsorption at −196 °C using a Quantachrome Autosorb-1 instrument.

Temperature-programmed reduction and oxidation (TPR/TPO) experiments were performed in a conventional flow system equipped with a mass spectrometer [15,19]. The reducibility of all samples was examined by TPR experiments in the temperature range of 25–650 °C, using 50-mg catalyst samples. Each sample was pretreated at 400 °C for 30 min under air flow before TPR. After cooling to room temperature under He, TPR experiments were carried out under a flow of a 3% H_2/He mixture (50 cm^3 min^{-1}) at a heating rate of 10 °C min^{-1}. Eleven sequential TPR/TPO cycles were performed over the $Cu_{0.30}Mn_{0.70}$ catalyst in the temperature range of 25–550 °C. TPR experimental conditions were the same as above, whereas in TPO experiments a flow of 1% O_2/He (50 cm^3 min^{-1}) was used. TPR and TPO runs were followed by a soak at 550 °C until the MS signals returned to baseline levels. Then the catalyst bed was cooled to room temperature under a He flow. A mass spectrometer (Omnistar/Pfeiffer Vacuum) was used for online monitoring of effluent gases.

X-ray photoelectron spectra (XPS) of Cu–Mn catalysts were recorded with experiments carried out in a commercial ultra-high-vacuum system, equipped with a hemispherical electron energy analyzer (SPECS LH-10) and a twin-anode X-ray gun for XPS measurements. The base pressure was 5×10^{-10} mbar. A non-monochromatized MgK_α line at 1253.6 eV and an analyzer pass energy of 97 eV were used in all XPS measurements. The surface composition of Cu–Mn samples in terms of atomic

ratios was calculated using a Shirley-type background and empirical cross-sectional factors for XPS [20].

2.3. Catalytic activity

Activity and selectivity measurements for SRM and CSRM processes were carried out at atmospheric pressure in a fixed-bed reactor system as described previously [15,19]. The samples were pretreated in a flowing 20 vol% O_2/He mixture at 400 °C for 30 min. The catalyst weight was 0.3 g, and the total flow rate of the reaction mixture was 70 $cm^3\,min^{-1}$ ($W/F = 0.257\ g\,s\,cm^{-3}$). The reaction feed was 5% MeOH, H_2O/MeOH = 1.5 in SRM tests and 5% MeOH, H_2O/MeOH = 1.26, O_2/MeOH = 0.10 in CSRM tests. Helium was used as a diluent. The catalyst samples were reduced by exposure to the SRM or CSRM feed for 2 h at 320 °C, after which measurements were made by stepwise decrease of reaction temperature. Identical results were obtained when reduction was carried out using a 5% H_2/He mixture instead of the (C)SRM feed. The catalytic performance of $Cu_{0.30}Mn_{0.70}$ catalyst also was examined for the SRM and CSRM processes with more concentrated feeds. A commercial Cu–Zn–Al catalyst (Haldor Topsoe LTS catalyst; Cu content 40 wt%) was used as a reference. Product and reactant analyses were carried out using a Shimadzu GC-14B gas chromatograph equipped with thermal conductivity and flame ionization detectors and Porapak QS and Carboxen columns. Helium was used as the GC carrier gas. H_2, CO_2, and CO were the main products of the SRM and CSRM reactions. Trace amounts of organic byproducts (formaldehyde and methyl formate) also were detected at low reaction temperatures. The H_2 and CO selectivities were calculated as

$$H_2\ \text{selectivity} = [CO_2]_{out}/\big([CO]_{out} + [CO_2]_{out}\big) \quad (5)$$

and

$$\text{CO selectivity} = [CO]_{out}/\big([CO]_{out} + [CO_2]_{out}\big). \quad (6)$$

Kinetic experiments were carried out under differential conditions (methanol conversion < 10%) using 50 mg of the $Cu_{0.30}Mn_{0.70}$ catalyst.

3. Results and discussion

3.1. Catalyst characterization

The specific surface area of combustion-prepared, copper–manganese oxide catalysts was found to be rather low, in agreement with previous studies [18,21]. More specifically, the specific surface areas of the catalysts were $Cu_{0.10}Mn_{0.90}$, 5 $m^2\,g^{-1}$; $Cu_{0.20}Mn_{0.80}$, 7 $m^2\,g^{-1}$; $Cu_{0.30}Mn_{0.70}$, 8 $m^2\,g^{-1}$; $Cu_{0.40}Mn_{0.60}$, 8 $m^2\,g^{-1}$; and $Cu_{0.50}Mn_{0.50}$, 7 $m^2\,g^{-1}$. Tanaka et al. [21] reported similar surface area values for Cu–Mn catalysts prepared by various methods and calcined at 700 °C for 10 h. Pure CuO and Mn_2O_3 had specific surface areas of 1 and 9 $m^2\,g^{-1}$, respectively.

3.1.1. XRD measurements

Fig. 1a shows XRD patterns of fresh Cu–Mn catalysts. The pure oxides were identified as CuO and Mn_2O_3, with the latter present in both cubic and orthorhombic phases, in agreement with other studies [22,23]. On the other hand, the spinel phase of $Cu_{1.5}Mn_{1.5}O_4$ was predominant in the mixed oxide samples and was already present in the sample with the lowest copper content ($Cu_{0.10}Mn_{0.90}$), as evidenced by the peak at ∼36°. The intensity of XRD peaks of the $Cu_{1.5}Mn_{1.5}O_4$ phase increased with copper content, whereas those of the Mn_2O_3 phase decreased. A small amount of Mn_2O_3 appeared to be present even at a Cu/(Cu + Mn) ratio of 0.40. Further increases in copper loading resulted in the disappearance of the Mn_2O_3 phase and appearance of the CuO phase in the XRD pattern. Li et al. [24] also found that the excess of copper or manganese led to the formation of CuO or Mn_2O_3 phase, respectively.

XRD analysis of used Cu–Mn catalysts after testing under CSRM conditions at 200–320 °C for ∼6 h showed that the spinel phase decomposed to MnO, Cu_2O, and Cu^0 phases (Fig. 1b). Detection of small amounts of oxidized copper species (Cu_2O) may result from partial reoxidation due to exposure to air. The intensity of XRD peaks of Cu^0 and Cu_2O phases increased with increasing copper content. Comparing the XRD patterns shown in Figs. 1a and 1b demonstrates that the used catalysts were less crystalline than the fresh ones. The XRD patterns of the $Cu_{0.30}Mn_{0.70}$ catalyst in (a) fresh condition and after testing under (b) SRM and (c) CSRM conditions are shown in Fig. 2. The phases identified after reaction correspond to decomposition/reduction of the spinel phase, as reported previously [25–27]. Table 1 summarizes the identified phases in the $Cu_{0.30}Mn_{0.70}$ catalyst and their corresponding JCPDS file numbers.

3.1.2. TPR measurements

The reducibility of Cu–Mn catalysts was investigated via TPR measurements. TPR profiles of all samples are shown in Fig. 3. Pure CuO was reduced to metallic copper in a single step and in the temperature range of 250–350 °C with a peak at 330 °C. This is a typical temperature range for CuO reduction [19,22,23,28,29]. The reduction profile of pure Mn_2O_3 was characterized by a broad low-temperature shoulder at 300–500 °C, followed by a peak at ∼520 °C. Reduction continued at temperatures as high as 600 °C. Generally, a two-step reduction profile of pure Mn_2O_3 has been reported [22,23,28]. Before formation of the MnO phase, Mn_2O_3 is reduced to Mn_3O_4 at lower temperatures. Further reduction of MnO to metallic manganese does not occur up to 1000 °C for thermodynamic reasons [29].

The reduction profiles of Cu–Mn catalysts were characterized by a main peak at ∼400 °C, which was present in all cases (Fig. 3). The intensity of this peak was similar for all catalysts except $Cu_{0.10}Mn_{0.90}$, for which it was lower. An additional peak appeared at 290–330 °C in the $Cu_{0.40}Mn_{0.60}$ and $Cu_{0.50}Mn_{0.50}$ catalysts, whose intensity increased with increasing copper content. Tanaka et al. [28] reported on the TPR profile of a Cu–Mn spinel oxide catalyst (Cu/Mn = 1/2, calcined at 900 °C), which is similar in shape and position to what was found in the present work for the $Cu_{0.30}Mn_{0.70}$ sample. Buciuman et al. [22] also

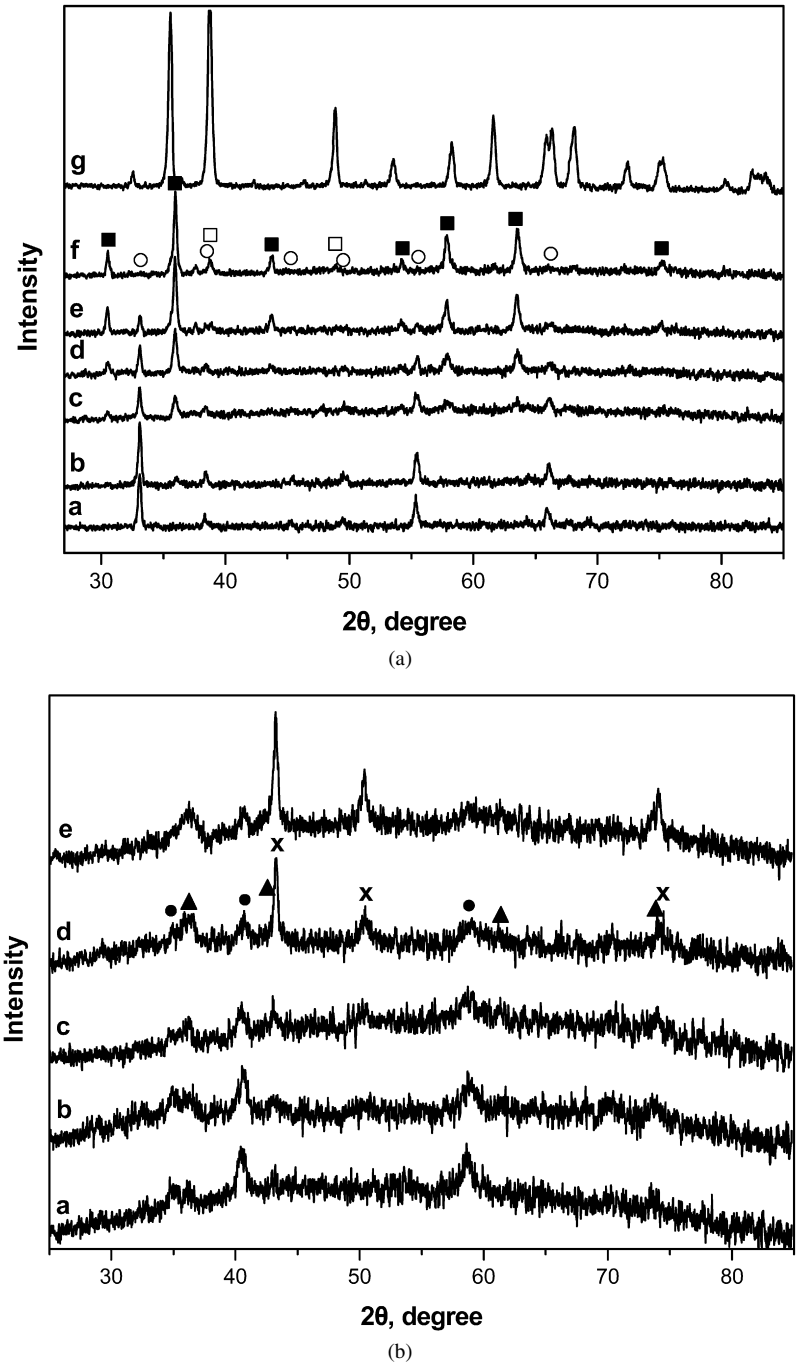

Fig. 1. (a) XRD patterns of as-prepared CuO, Mn_2O_3 and Cu–Mn catalysts. (a) Mn_2O_3, (b) $Cu_{0.10}Mn_{0.90}$, (c) $Cu_{0.20}Mn_{0.80}$, (d) $Cu_{0.30}Mn_{0.70}$, (e) $Cu_{0.40}Mn_{0.60}$, (f) $Cu_{0.50}Mn_{0.50}$ and (g) CuO. (■) $Cu_{1.5}Mn_{1.5}O_4$, (○) Mn_2O_3, (□) CuO. (b) XRD patterns of Cu–Mn catalysts after CSRM. (a) $Cu_{0.10}Mn_{0.90}$, (b) $Cu_{0.20}Mn_{0.80}$, (c) $Cu_{0.30}Mn_{0.70}$, (d) $Cu_{0.40}Mn_{0.60}$, (e) $Cu_{0.50}Mn_{0.50}$. (▲) Cu_2O, (●) MnO, (**X**) Cu^0.

observed that Cu–Mn spinel prepared at 1000 °C is reduced with a peak at 410 °C. On the other hand, other previous reports [23,26,30] have indicated that the spinels (Cu/Mn = 1/1 or 1/2, T_{calc} = 500–550 °C) are reduced in the temperature range of 200–350 °C. The origin of this discrepancy is not quite clear. One possibility is differences in the surface area of the catalysts; the samples in Refs. [23,26,30], which had surface areas in the range of 18–33 $m^2\,g^{-1}$, were reduced at lower temperatures than the samples in Refs. [22,28], which had surface areas <1 $m^2\,g^{-1}$. Our samples had also rather low surface areas, in the range of 5–8 $m^2\,g^{-1}$. Tanaka et al. [28] examined the effect of calcination temperature on the surface area and reducibility of Cu–Mn spinel catalysts and found that the surface area of spinel catalysts decreased from 6.6 to 0.6 $m^2\,g^{-1}$ with an increase in calcination temperature from 500 to 1100 °C, but the peak temperature in the TPR profiles did not change; that is, there was no effect on reducibility. Buciuman et al. [22], on the other hand, found that an increase in calcination temperature from 550 to 1000 °C led to a decrease in surface area from 2.6 to 0.7 $m^2\,g^{-1}$ and a shift of TPR peak temperature from 320 to

410 °C. Our TPR results are comparable to those obtained for low-surface area samples prepared by calcination at high temperatures. It should be recalled that high temperatures of the order of 1000 °C developed, albeit for a few seconds, during the combustion synthesis used in the present work.

The appearance of a low-temperature TPR peak at ∼290–330 °C for the copper-rich catalysts ($Cu_{0.40}Mn_{0.60}$ and $Cu_{0.50}Mn_{0.50}$) may be attributed to reduction of CuO species, not incorporated into the spinel lattice. This is based on the following evidence: (i) The position of this peak is similar to the one of pure CuO reduction; (ii) the intensity of this peak increases with increase of copper content; and (iii) XRD patterns of $Cu_{0.40}Mn_{0.60}$ and $Cu_{0.50}Mn_{0.50}$ catalysts indicate the presence of a CuO phase.

The TPR results of Cu–Mn catalysts indicate that manganese ions are reduced at lower temperatures compared with pure Mn_2O_3. It is generally accepted that copper has a promoting effect on the reduction of manganese ions in the spinel catalyst [23,26,28,30]. It is also evident in Fig. 3 that reduction of $Cu_{0.10}Mn_{0.90}$, $Cu_{0.20}Mn_{0.80}$, and $Cu_{0.30}Mn_{0.70}$ catalysts commences at a lower temperature than that of pure CuO. This implies that the initiation of reduction of copper ions is also promoted by the presence of manganese ions.

Table 1
Crystalline phases of $Cu_{0.30}Mn_{0.70}$ catalyst

Catalyst status	Crystalline phases (JCPDS file No.)
As-prepared	$Cu_{1.5}Mn_{1.5}O_4$ (35-1171) Mn_2O_3 (cubic, 41-1442) Mn_2O_3 (orthorhombic, 24-0508)
After SRM	MnO (07-0230) Mn_3O_4 (24-0734) γ-Mn_2O_3 (tetragonal, 06-0540) Cu^0 (04-0836)
After CSRM	MnO (07-0230) Cu_2O (03-0892) Cu^0 (04-0836)

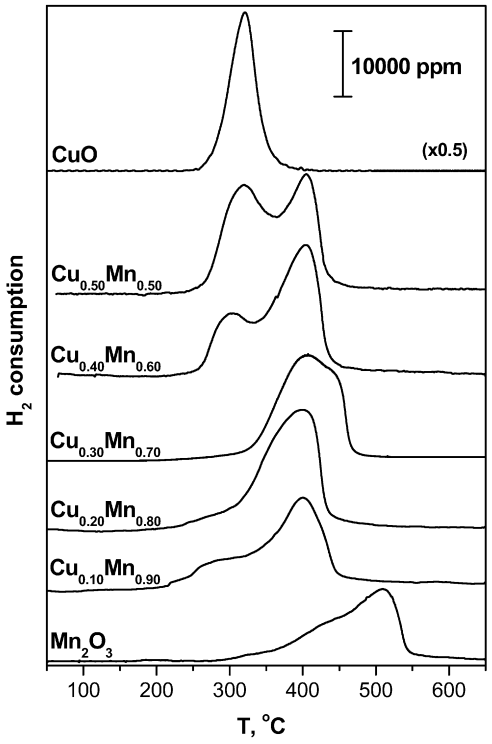

Fig. 3. H_2-TPR profiles of as-prepared CuO, Mn_2O_3 and Cu–Mn catalysts.

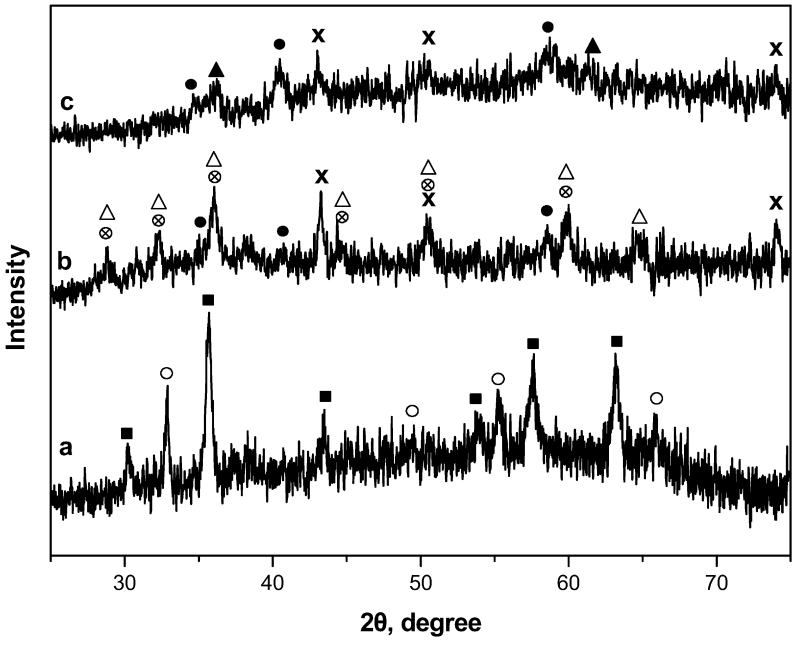

Fig. 2. XRD patterns of $Cu_{0.30}Mn_{0.70}$ catalyst (a) as-prepared, (b) after SRM and (c) after CSRM. (■) $Cu_{1.5}Mn_{1.5}O_4$, (○) Mn_2O_3, (▲) Cu_2O, (●) MnO, (**X**) Cu^0, (△) Mn_3O_4, (⊕) γ-Mn_2O_3.

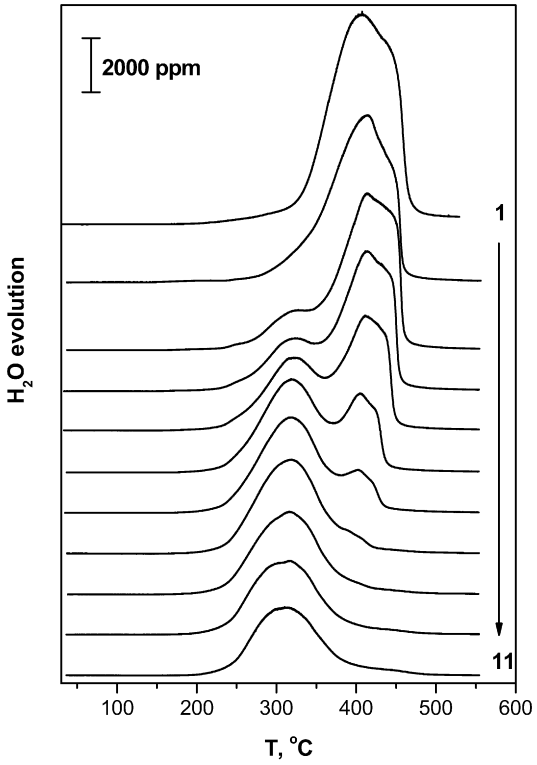

(a)

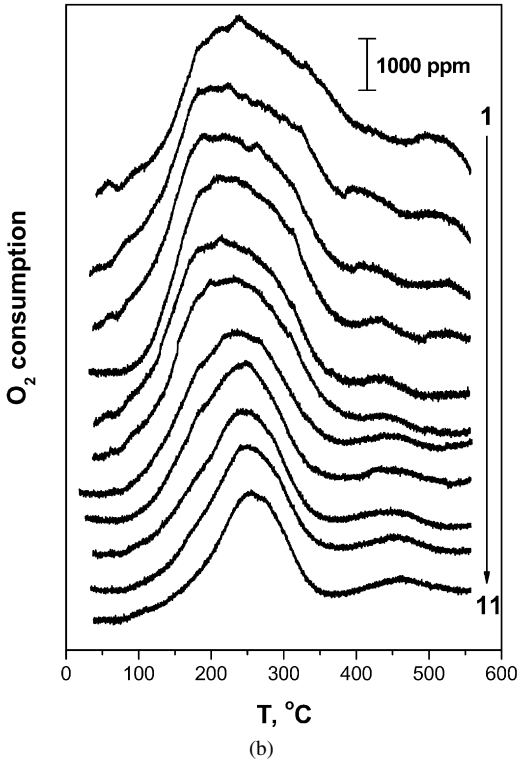

(b)

Fig. 4. TPR/TPO cycles (from 1 to 11) of $Cu_{0.30}Mn_{0.70}$ catalyst.

3.1.3. Redox cycles

Successive TPR/TPO runs were carried out over the $Cu_{0.30}Mn_{0.70}$ catalyst to examine the reversibility of reduction/oxidation cycles. The maximum temperature of the runs was the same as used in catalyst synthesis (550 °C) to avoid temperature-induced changes in catalyst structure. The sequential TPR and TPO profiles are shown in Figs. 4a and 4b, respectively, and the amounts of H_2 or O_2 consumption in each cycle are presented in Fig. 5. Significant changes can be observed in the reduction profiles of sequential TPR runs. Each profile can be divided into 2 overlapping regions: (i) region I, in the temperature range of 350–480 °C, which is characterized by a main peak at 400 °C, accompanied by a high-temperature shoulder at 430–460 °C. The intensity of this peak gradually decreases and vanishes after the ninth run, (ii) region II in the temperature range of 220–380 °C, which is characterized by a single symmetrical peak at ∼320 °C. This peak develops after the third cycle, gradually increases in intensity and essentially stabilizes after the ninth cycle.

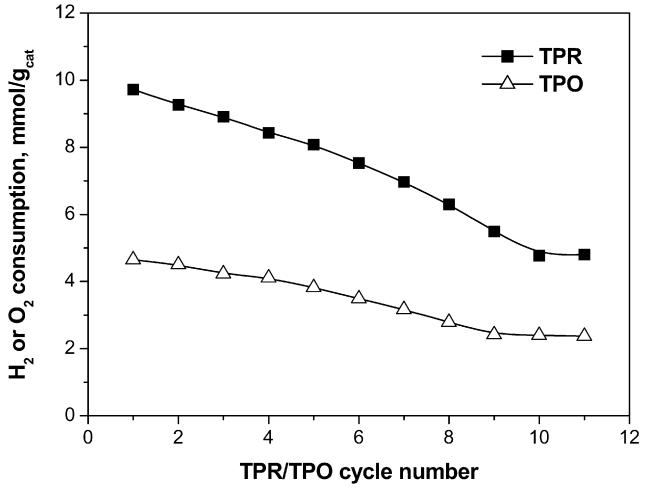

Fig. 5. Hydrogen and oxygen uptake during TPR/TPO cycles.

The amount of hydrogen consumed during TPR (Fig. 5) progressively decreased in successive TPR runs and remained practically unchanged after the ninth run. The amount of H_2 consumed in the first runs is slightly higher than the one corresponding to reduction of both CuO (to Cu^0) and Mn_2O_3 (to MnO) at the specific composition of the $Cu_{0.30}Mn_{0.70}$ catalyst. This means that complete reduction of the spinel phase occurs during TPR and the excess consumption of hydrogen may be attributed to (i) the presence of Mn^{4+} ions and (ii) hydrogen incorporation in the catalyst during TPR. Hydrogen incorporation during TPR was confirmed by carrying out a TPD run right after TPR, during which desorption of small amounts of H_2 was observed (1–2% of the amount of H_2 consumed during TPR). The amount of hydrogen consumed in the last cycles indicates that mostly CuO reduction occurs.

The profiles of successive TPO runs (Fig. 4b), which followed after each TPR run, are characterized by a main peak at 200–300 °C and a broad feature above 400 °C. With an increase in cycle number, the intensity of the TPO profile decreases, but otherwise no significant change is observed in the profile appearance. The amount of oxygen consumed (Fig. 5) gradually decreased in a similar fashion to that of hydrogen during successive TPO cycles, and its quantity was approximately half of that of hydrogen as expected from the stoichiometries of reduction and oxidation. The results obtained in the TPR/TPO cycles

indicate that the efficiency of spinel reformation was diminished at successive reduction/oxidation cycles; that is, oxidation at temperatures up to 550 °C was not sufficient to fully restore the spinel structure. It should be emphasized that the TPR profiles at high cycle numbers were quite similar to that of pure CuO, which implies that during TPO, Cu^0 is oxidized to Cu^{2+}, but copper ions are not incorporated back to the spinel structure. This might be due to increasing difficulty of MnO reoxidation at successive cycles. The amounts of O_2 consumed in the last cycles correspond to full oxidation of Cu^0 to CuO and oxidation of only a small percentage (20%) of Mn^{2+} to Mn^{3+}. Oku et al. [31] reported that the surface of MnO is not easily oxidized at temperatures below 600 °C.

The amount of hydrogen consumed during TPR corresponds to reduction of the catalysts toward Cu^0 and MnO. Therefore, the catalyst structure after a TPR run should be analogous to that after a methanol-reforming test for which XRD analysis (Fig. 2) showed that the spinel oxide phase is decomposed under the reducing conditions of reforming with copper segregation on the catalyst surface. Tanaka et al. [27,28] concluded, based on TPR and XRD measurements, that reduction of Cu–Mn spinel oxides leads to formation of highly dispersed Cu species that contribute to high CO conversion in the WGS reaction. A sequential reduction/oxidation treatment was applied by Paldey et al. [29] to improve the catalytic activity of a Cu–Mn–Fe pigment in the CO oxidation reaction. Their findings indicate that reoxidation leads to formation of small clusters of the spinel phase around small Cu and MnO domains. This refined morphology with high density of defects led to great enhancement of CO oxidation activity.

3.1.4. XPS measurements

The oxidation states of copper and manganese in the spinel oxide catalysts were determined via XPS surface analysis. Surface atomic ratios were also calculated and compared with bulk ratios. These measurements are summarized in Table 2. Fig. 6 compares the Mn 2p and Cu 2p binding energies and Cu L_3VV Auger kinetic energy of Cu–Mn spinel oxides. XPS curve-fitting analysis revealed that Mn(III), Mn(IV), Cu(II), and Cu(I) species are simultaneously present in the fresh, oxidized samples. Although the interpretation of XPS spectra of manganese oxides in terms of the actual Mn oxidation state is complex due to the slight differences of the corresponding binding energies of the main peaks, the peak at 642 eV (Fig. 6A) can be assigned to Mn^{3+} and Mn^{4+} cations, in agreement with previous reports [32–38]. A binding energy equal or higher than 642 eV reveals the presence of both cations; a slightly higher binding energy is observed when Mn^{4+} alone is present [35,36]. The fact that the Mn 2p spectra do not contain any shake-up features at higher binding energies suggests the absence of Mn^{2+} species from the catalyst surface [31,39,40].

Copper in all of the as-prepared samples had its $2p_{3/2}$ (Fig. 6B) main peak located at ∼933.9 eV. In accordance with previous studies, this peak is assigned to Cu^{2+} cations, because it is accompanied by a strong shake-up line at ∼942 eV [19,26,33,37,38,40]. The relative intensity of the satellite with respect to the main line was estimated to be in the range of 0.27 ($x = 0.50$)–0.83 ($x = 0.10$). The corresponding values for pure CuO and Cu_2O are 0.55 and 0 [19]. An additional peak shoulder appeared at 931 eV for copper loadings above $x = 0.10$, the intensity of which increased with copper loading. The lower binding energies at ca. 932 eV suggest the presence of reduced copper species; however, the Cu $2p_{3/2}$ binding energies cannot be used to distinguish between Cu^+ and Cu^0, because these were almost identical. The corresponding kinetic energy spectra of Cu L_3VV electron (Fig. 6C) consisted of a main peak at 916.7 eV, indicating the absence of Cu^0. Jernigan and Somorjai [41] found kinetic energies of 918.5 eV for Cu^0, 916.5 eV for Cu_2O, and 917.6 eV for CuO. In addition, the calculated values of the Auger parameter, α, were ∼1851.7 and ∼1848.8, characteristic of the presence of Cu^{2+} and Cu^+ species, respectively. Thus, the peak at 931 eV in the Cu 2p XP spectra can be attributed to Cu^+. The binding energy of Cu(I) is strongly negatively shifted, however. These experimental observations are in agreement with the formation of Cu^+ and Mn^{4+} ions as a result of the redox equilibrium $Cu^{2+} + Mn^{3+} = Cu^+ + Mn^{4+}$, which is expected on copper substitution. The results of the surface quantitative analysis (Table 2 and Fig. 7) show that a nearly homogeneous Cu–Mn composition between the surface and the bulk was obtained for catalysts with copper loading up to $x = 0.30$. Further increases in copper loading resulted in decreased copper dispersion, in agreement with XRD analysis, which revealed the presence of the CuO phase at higher copper loadings (i.e., $x = 0.50$). A similar linear increase in Cu^+ concentration also occurred with copper loading up to $x = 0.30$.

In accordance with XRD measurements, XPS analysis also revealed decomposition of the spinel oxide after the reforming test, with the Cu $2p_{3/2}$ peak shoulder at 931 eV disappearing.

Table 2
XPS analysis of fresh Cu–Mn catalysts

Catalyst	Cu $2p_{3/2}$ B.E., eV[a]		Cu L_3VV K.E., eV	Mn $2p_{3/2}$, B.E., eV[a]	Surface atomic ratio		
	Cu^{2+}	Cu^+			Cu/(Cu + Mn)	$Cu_{sat.}/Cu_{main}$[b]	$Cu^+/(Cu^+ + Cu^{2+})$
$Cu_{0.10}Mn_{0.90}$	933.9 (3.2)	–	917.8	642.0 (3.0)	0.12	0.83	0.00
$Cu_{0.20}Mn_{0.80}$	933.9 (3.2)	931.0 (2)	917.8	642.0 (3.2)	0.19	0.52	0.13
$Cu_{0.30}Mn_{0.70}$	933.8 (3.2)	931.0 (2)	917.8	641.9 (3.3)	0.24	0.62	0.21
$Cu_{0.40}Mn_{0.60}$	933.8 (3.2)	931.0 (2)	917.8	642.0 (3.2)	0.25	0.29	0.22
$Cu_{0.50}Mn_{0.50}$	933.9 (3.2)	931.0 (2)	917.5	641.9 (3.3)	0.28	0.29	0.25

[a] FWHM in parenthesis.
[b] Cu_{main}: Cu $2p_{3/2}$ main line, $Cu_{sat.}$: Cu $2p_{3/2}$ satellite.

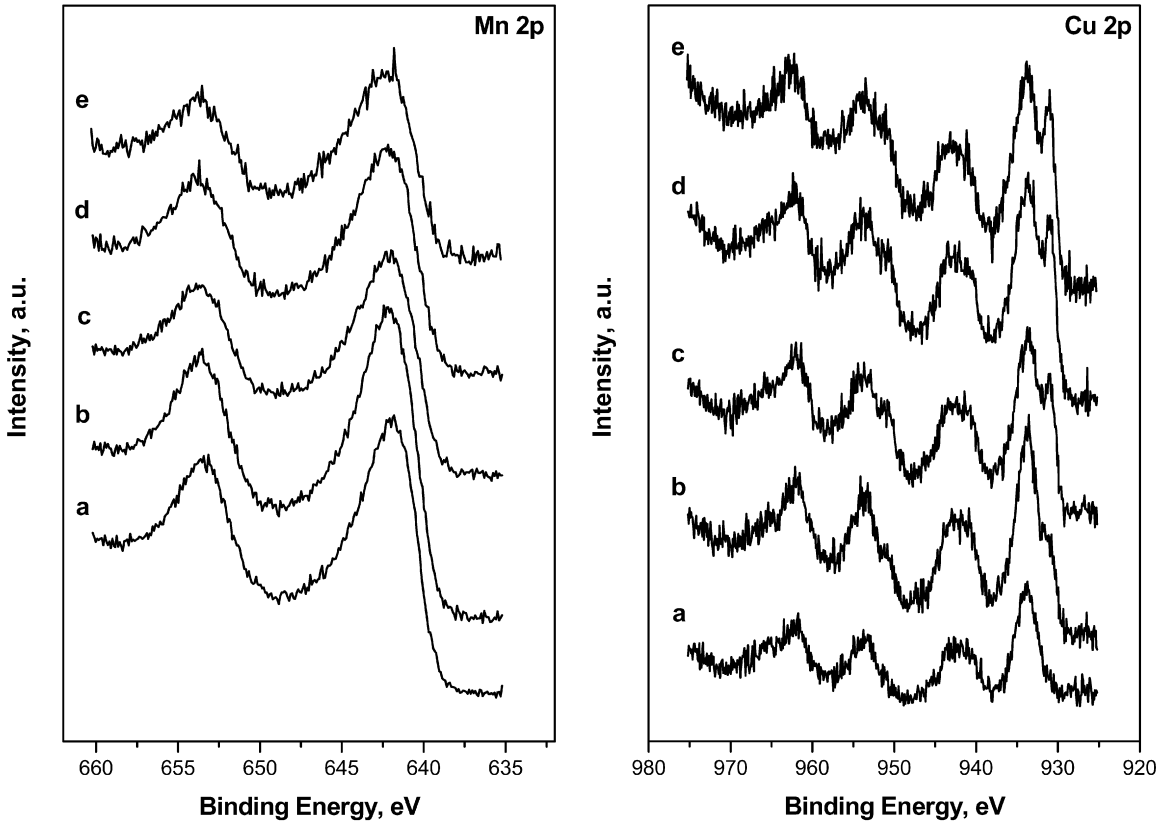

Fig. 6. (A) Mn 2p XP spectra, (B) Cu 2p XP spectra and (C) kinetic energy spectra of Cu L_3VV Auger electron of Cu–Mn catalysts. (a) $Cu_{0.10}Mn_{0.90}$, (b) $Cu_{0.20}Mn_{0.80}$, (c) $Cu_{0.30}Mn_{0.70}$, (d) $Cu_{0.40}Mn_{0.60}$ and (e) $Cu_{0.50}Mn_{0.50}$.

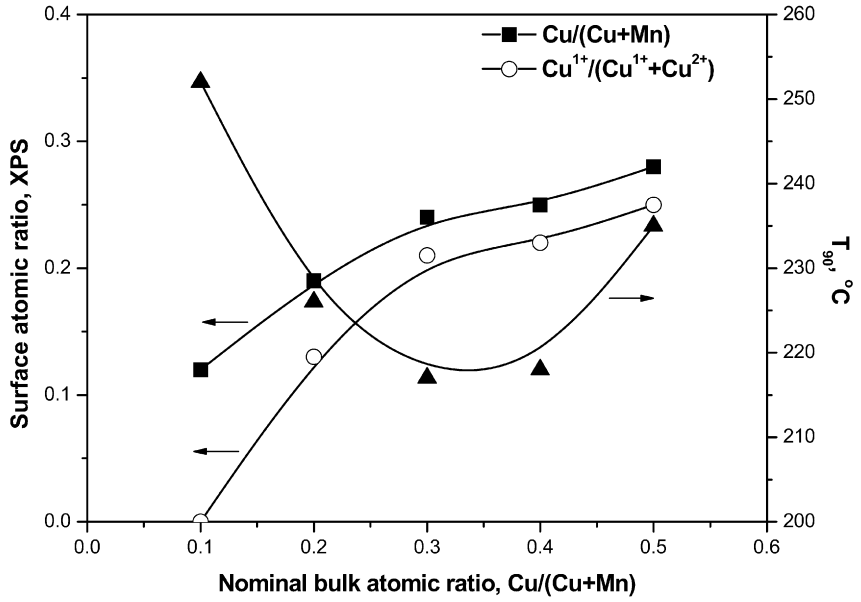

Fig. 7. Variation of the surface atomic ratios of Cu/(Cu + Mn) and $Cu^{+}/(Cu^{+} + Cu^{2+})$ determined by XPS and of the temperature at which 90% conversion of methanol was obtained (CSRM process, Fig. 8) versus the corresponding nominal bulk ratio of Cu/(Cu + Mn).

This peak demonstrates the presence of copper ions in the spinel structure. On the other hand, further analysis of copper and manganese XPS spectra in spent catalysts was difficult due to the possibility of surface reoxidation after exposure in air before the XPS measurements.

3.2. Catalytic activity and selectivity

The catalytic activity and selectivity of Cu–Mn catalysts for the CSRM process are shown in Fig. 8. Catalyst activity increased with increasing copper content, up to $x = 0.40$. Further increases in copper loading led to decreased catalytic activity. The similar performance of $Cu_{0.30}Mn_{0.70}$ and $Cu_{0.40}Mn_{0.60}$ is closely related to their almost identical physicochemical characteristics, as shown in their XRD patterns (Fig. 1a) and the XPS analysis (Table 2 and Fig. 7). As shown in Fig. 7, the catalytic activity, expressed as the temperature at which 90% conversion of methanol is achieved (T_{90}) increased (i.e., decrease in T_{90} value) monotonically with the surface concentration of well-dispersed copper species. T_{90} values were minimized in the range $x = 0.30$–0.40. Further increases in copper loading resulted in formation of bulk CuO and subsequent decreased catalytic activity. This is in line with TPR results (Fig. 3), which show that for $x > 0.30$, a low-temperature peak appeared in the TPR profiles, attributed to the reduction of surface copper oxide species (i.e., of copper ions not incorporated into the spinel structure). At the highest copper loading ($x = 0.50$), these CuO species are readily visible in the XRD pattern.

The most active samples ($Cu_{0.30}Mn_{0.70}$ and $Cu_{0.40}Mn_{0.60}$) exhibited almost identical activity and selectivity curves (Fig. 8) and achieved 100% methanol conversion with ~97% H_2 selectivity at 240 °C. CO selectivity was lower than its equilibrium value at reaction temperatures below 240 °C, whereas it was quite close to equilibrium at temperatures above 240 °C, where methanol conversion was 100%. Hutchings et al. [42] reported

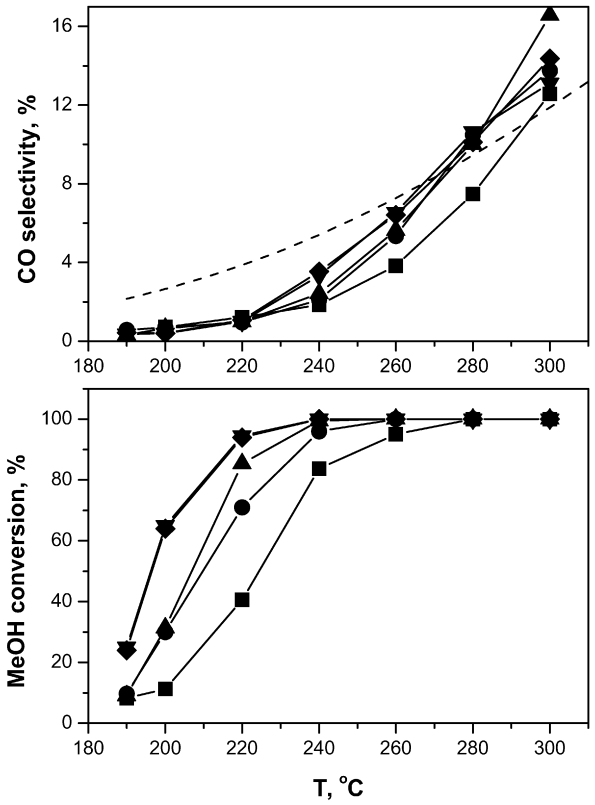

Fig. 8. Effect of Cu/(Cu + Mn) ratio on activity and selectivity of Cu–Mn catalysts for the CSRM process. $W/F = 0.257$ g s cm^{-3}, 5% MeOH, H_2O/MeOH = 1.26, O_2/MeOH = 0.10. (■) $Cu_{0.10}Mn_{0.90}$, (▲) $Cu_{0.20}Mn_{0.80}$, (▼) $Cu_{0.30}Mn_{0.70}$, (◆) $Cu_{0.40}Mn_{0.60}$, (●) $Cu_{0.50}Mn_{0.50}$. Dashed line: equilibrium CO selectivity.

that Cu–Mn catalysts prepared with a Cu/Mn ratio > 1 showed similar catalytic activity for the oxidation of CO; nevertheless, the Mn-rich catalysts were much more active, and the sample

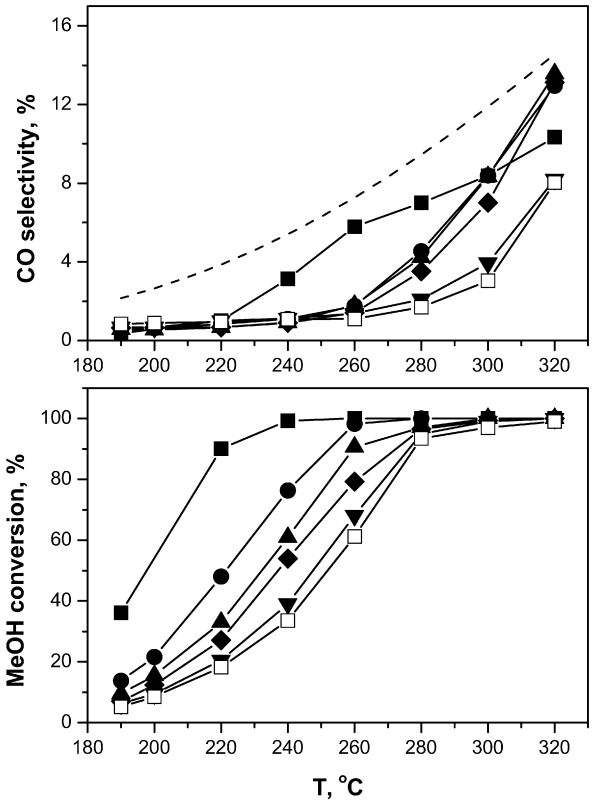

Fig. 9. Effect of MeOH concentration on activity and selectivity of $Cu_{0.30}Mn_{0.70}$ catalyst for SRM process. $W/F = 0.257\ g\,s\,cm^{-3}$, $H_2O/MeOH = 1.5$. (■) 5% MeOH, (●) 10% MeOH, (▲) 15% MeOH, (◆) 20% MeOH, (▼) 25% MeOH, (□) 31.8% MeOH. Dashed line: equilibrium CO selectivity.

with Cu/Mn = 0.47 [i.e., Cu/(Cu + Mn) = 0.32] was the most active of all.

3.2.1. Kinetic analysis

Fig. 9 illustrates the effect of methanol concentration in the catalytic performance of the selected $Cu_{0.30}Mn_{0.70}$ catalyst. With an increase in the methanol partial pressure in the feed, the methanol conversion decreased, implying a reaction order <1 with respect to methanol partial pressure, in agreement with previous results [43]. Using a feed with 31.8% MeOH, a conversion of 93.5% was obtained at 280 °C with 98.3% H_2 selectivity. CO selectivity decreased with increasing methanol concentration in the feed and in all cases was lower than its corresponding equilibrium value.

To examine the effect of water and methanol partial pressure on the SRM reaction, additional experiments were performed under differential reaction conditions. These experiments were conducted with fixed methanol and varying water partial pressure and vice versa. With an increase of water or methanol partial pressure, the reaction rate of CO_2 production increased, as shown in Fig. 10. The kinetic data were fitted by a simple power law expression [44]

$$-r_{MeOH} = k_0 \exp(-E/RT)\, P_{MeOH}^{a} P_{H_2O}^{b}. \quad (7)$$

The kinetic parameters—pre-exponential factor, k_0, activation energy, E, and the reaction orders a and b—obtained by fitting the experimental data were $a = 0.7$, $b = 0.5$, $E = 71\ kJ\,mol^{-1}$, and $k_0 = 6.33 \times 10^9\ \mu mol\,g^{-1}\,s^{-1}\,atm^{-1.2}$.

The solid lines in Fig. 10 correspond to the predictions of Eq. (7) using the above values of the kinetic parameters. A quite satisfactory fitting of experimental results was obtained in all cases. The apparent activation energy of methanol reforming over Cu–Zn-based catalysts has been reported to be in the range of 75–105 kJ mol^{-1} [43–48]. There are no literature results concerning Cu–Mn catalysts. Idem and Bakhshi [50] have reported an activation energy of ∼79 kJ mol^{-1} for Cu–Al–Mn catalysts. Therefore, the activation energy found in this work lies on the left-hand side of reported values. It should be noted that the catalyst particle size used in this work is sufficiently small to allow any mass/heat transfer effect on the kinetic results to be ruled out. The reaction orders with respect to methanol and water partial pressure have been determined by many investigators, mainly for Cu–Zn catalysts [43,46,48]. The reported values are generally in the range of 0.2–0.6 for methanol and 0.02–0.4 for water; these values are comparable to what we found in the present work for the Cu–Mn catalysts. The overall reaction order of methanol reforming with respect to reactants was 1.2 (0.7 + 0.5), which implies that methanol conversion should not be significantly influenced by increased methanol and water concentration in the feed. In the actual experiment, however, the conversion of methanol decreased considerably with increasing methanol and water concentration in the feed (Fig. 9). This is attributed to inhibition of the reaction by produced hydrogen. In many cases, a negative reaction order with respect to hydrogen partial pressure has been reported [43,46,48]; in addition, one article has reported a negative reaction order for carbon dioxide [47]. It also should be noted that during the differential kinetic experiments, the sole carbon-containing product was CO_2, whereas CO also was produced in integral tests, especially at high temperatures. If CO were a primary product of the reaction, then CO concentration in the products would be equal to or greater than the corresponding CO concentration at the WGS equilibrium. Because the CO concentration was always well below the equilibrium CO concentration, it is safe to assume that CO_2 was the primary product of methanol steam reforming and that CO was produced as a secondary product via the reverse WGS reaction. If CO were produced through the Boudouard reaction [49,50], then signs of early deactivation should be evident due to carbon deposition. Combustion-synthesized Cu–Mn catalysts showed no signs of deactivation during catalytic activity runs, whereas very low amounts of CO_2 were produced during TPO runs (not shown) carried out immediately after methanol-reforming experiments.

3.2.2. CSRM versus SRM

The activity and selectivity curves for both SRM and CSRM over the $Cu_{0.30}Mn_{0.70}$ catalyst are shown in Fig. 11. The methanol conversion curves obtained under SRM and CSRM conditions were similar in the case of the diluted feed (5% MeOH). In contrast, significantly enhanced methanol conversion was observed under CSRM conditions in the case of the concentrated feed (31.8% MeOH). The T_{50} was 250 °C for the SRM process and 210 °C for the CSRM process. We previ-

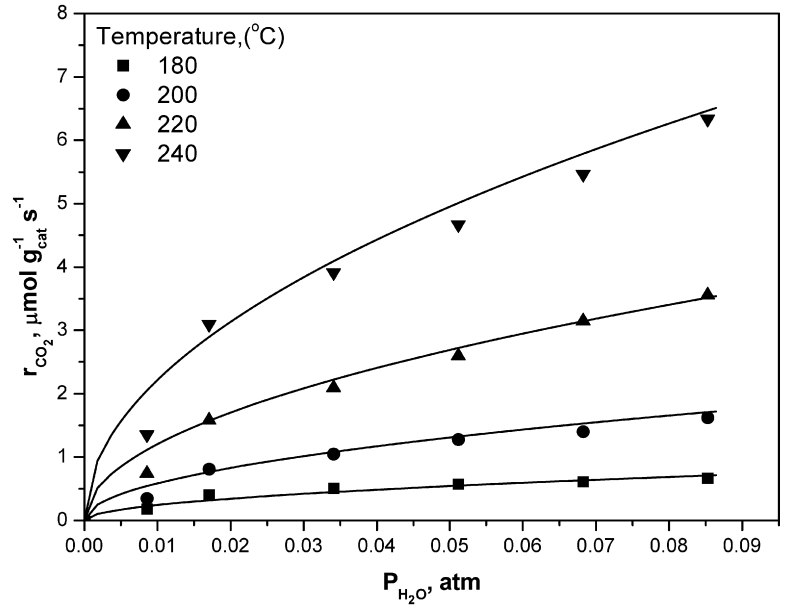

(a)

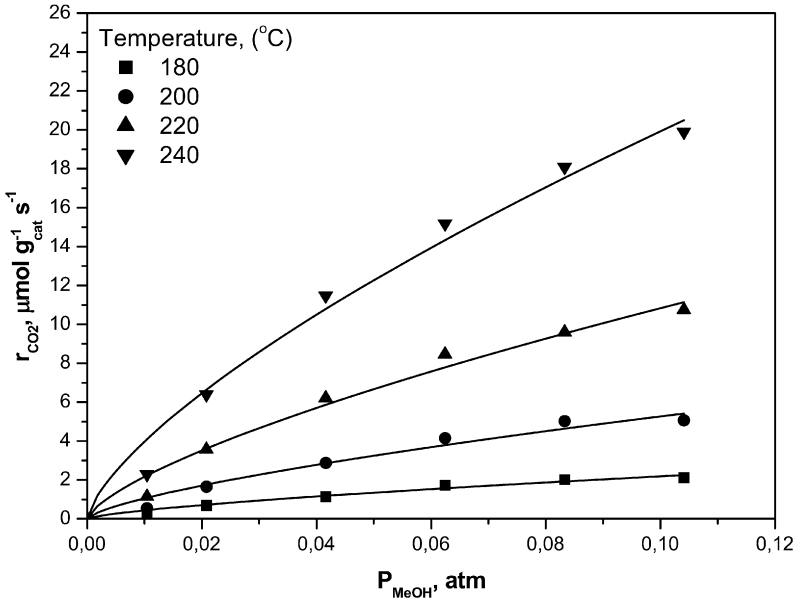

(b)

Fig. 10. Reaction rate of steam reforming of methanol as a function of (a) water partial pressure at $P_{MeOH} = 0.02$ atm and (b) methanol partial pressure at $P_{H_2O} = 0.085$ atm, over the $Cu_{0.30}Mn_{0.70}$ catalyst. Symbols: experimental points. Solid lines: model predictions according to Eq. (7).

ously reported [15], in accordance with other groups [3,4,12, 13], that the improved catalytic activity for methanol reforming by co-feeding oxygen along with steam and methanol may be attributed to more efficient heat transfer in the catalytic bed, because oxygen is initially consumed through combustion of part of methanol feed and heat is generated in situ in the direction of flow. It is understandable that this heat effect should be more pronounced in the case of the concentrated feed, which contains more oxygen than the diluted feed. Regarding CO selectivity, the curves of the SRM and CSRM processes were almost identical (with the exception of 5% MeOH in the feed) above 260 °C, whereas any further increase in reaction temperature resulted in increased CO selectivity in the case of the CSRM process.

3.2.3. *Cu–Mn spinel oxide versus commercial $Cu/ZnO/Al_2O_3$ catalyst*

The catalytic performance of the $Cu_{0.30}Mn_{0.70}$ catalyst was compared with that of a commercial $Cu/ZnO/Al_2O_3$ reforming catalyst under identical reaction conditions. The conversion and selectivity curves of SRM and CSRM processes over these 2 catalysts are shown in Fig. 12. In the case of steam reforming with dilute feed (5% MeOH, Fig. 12a), the catalytic performance of these catalysts was almost identical in both the presence and absence of oxygen. When a concentrated feed (31.8% MeOH, Fig. 12b) was used, the two catalysts exhibited similar activity in the presence of oxygen, but the commercial catalyst was more active than $Cu_{0.30}Mn_{0.70}$ in the absence of

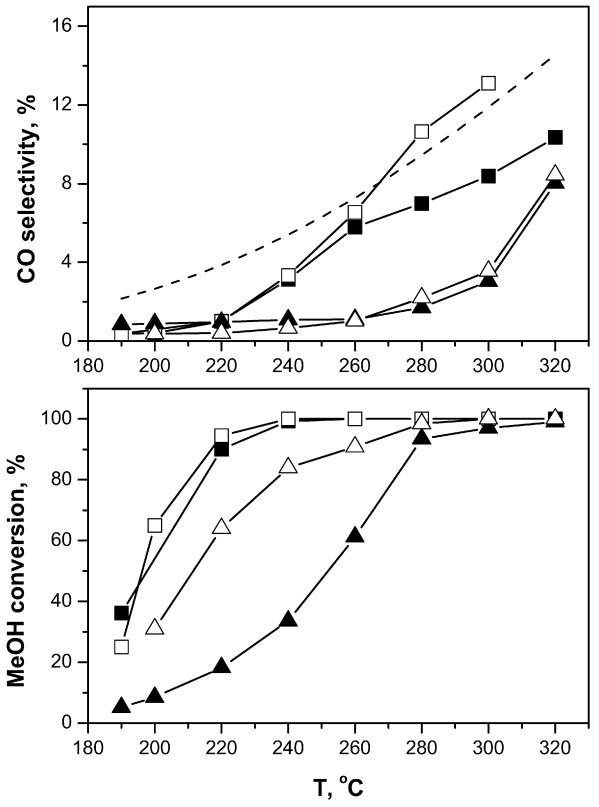

(a)

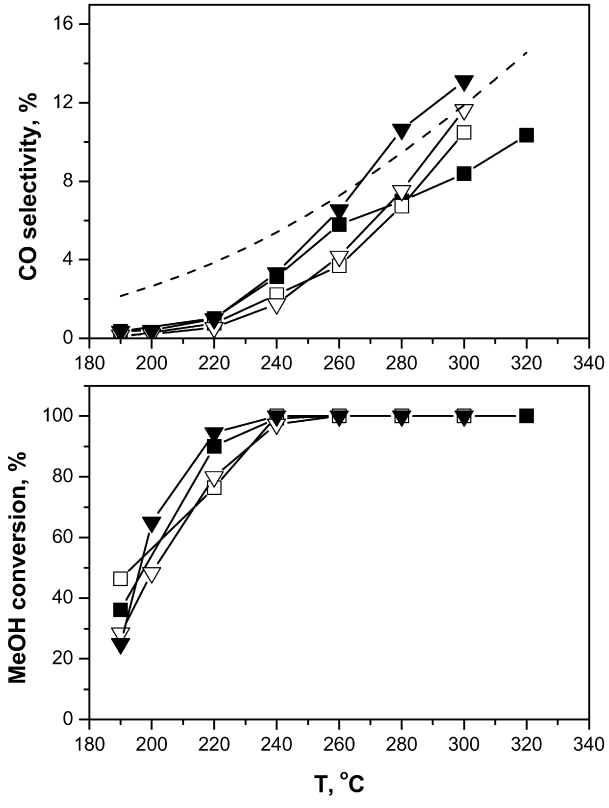

(b)

Fig. 11. MeOH conversion and CO selectivity over the $Cu_{0.30}Mn_{0.70}$ catalyst, for SRM (solid symbols) and CSRM (open symbols) processes, with (■) 5% MeOH and (▲) 31.8% MeOH. SRM: H_2O/MeOH = 1.5, CSRM: H_2O/MeOH = 1.26, O_2/MeOH = 0.10.

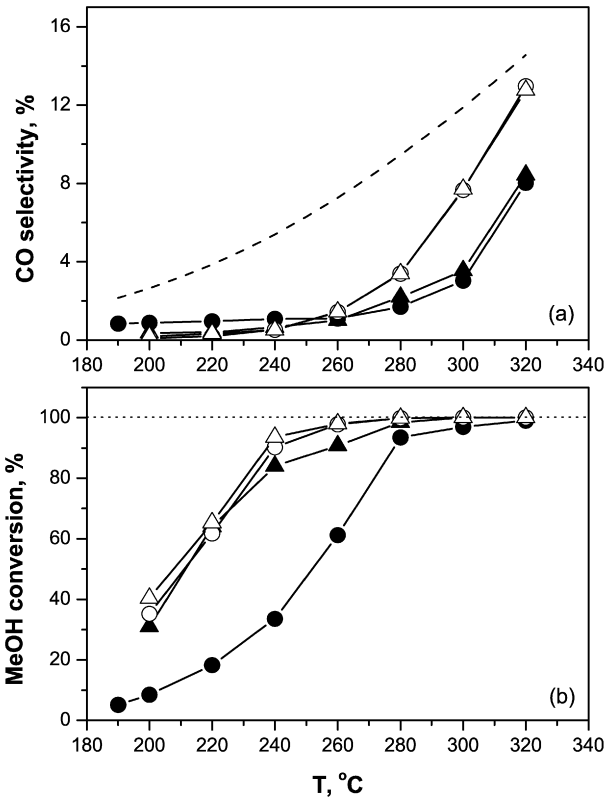

Fig. 12. Comparison between $Cu_{0.30}Mn_{0.70}$ (solid symbols) and commercial (open symbols) catalysts, for different feedstreams: (a) (●) SRM (5% MeOH, H_2O/MeOH = 1.5) and (▲) CSRM (5% MeOH, H_2O/MeOH = 1.26, O_2/MeOH = 0.10). (b) (●) SRM (31.8% MeOH, H_2O/MeOH = 1.5) and (▲) CSRM (31.8% MeOH, H_2O/MeOH = 1.26, O_2/MeOH = 0.10). W/F = 0.257 g s cm^{-3}. Dashed line: equilibrium CO selectivity.

oxygen. The addition of oxygen did not seem to affect the performance of the commercial catalyst. Similar results regarding the effect of co-added oxygen on methanol conversion over Cu–Zn–Al catalysts have been reported by Agrell et al. [13] and Lindstrom et al. [51]. In contrast, the activity of the Cu–Mn catalyst was increased considerably by co-addition of O_2. The different response of the two catalysts on the addition of oxygen implies that, in addition to heat effects, oxygen may modify the oxidation state and activity of the catalysts. It also should be mentioned that the $Cu_{0.30}Mn_{0.70}$ catalyst exhibited lower CO selectivity than the commercial catalyst at high temperatures, where methanol conversion was close to 100%.

3.2.4. Stability with reaction time

One of the major problems associated with using copper-based catalysts in methanol reforming is the deactivation with time-on-stream, due mainly to copper sintering or formation of carbonaceous deposits on the catalyst surface [43–46,49,50,52]. To investigate the stability of Cu–Mn catalysts under CSRM reaction conditions compared with that of the commercial Cu–Zn–Al catalyst, 8-h catalytic runs were performed at 300 °C over the $Cu_{0.30}Mn_{0.70}$ and Cu–Zn–Al catalysts. The results, shown in Fig. 13, indicate that the only difference between the catalysts was in the H_2 selectivity, which was higher over the $Cu_{0.30}Mn_{0.70}$ catalyst (92.5 vs 85% over Cu–Zn–Al). Oth-

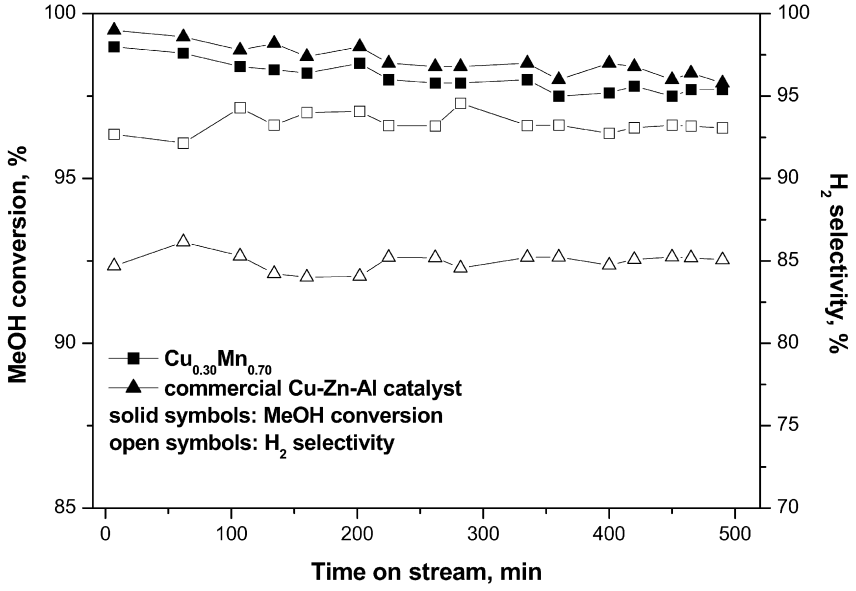

Fig. 13. Variation of methanol conversion (solid symbols) and H_2 selectivity (open symbols) with reaction time-on-stream for the CSRM over $Cu_{0.30}Mn_{0.70}$ and commercial Cu–Zn–Al catalysts. Operating conditions: $W/F = 0.257\ \mathrm{g\,s\,cm^{-3}}$, 31.8% MeOH, H_2O/MeOH = 1.26, O_2/MeOH = 0.10, $T = 300\,^{\circ}\mathrm{C}$.

erwise, the methanol conversion obtained over these catalysts was comparable, and the catalysts also appeared to be quite stable with decreasing methanol conversion from 98–99% to 96% after 8 h on stream. The H_2 selectivity remained practically unchanged throughout this period. Purnama et al. [44] reported a rapid decline within the first hours of steam reforming with a commercial $Cu/ZnO/Al_2O_3$ catalyst. A commercial $Cu/ZnO/Al_2O_3$ catalyst, Synetix 33-5 [43], also declined relatively quickly and became stable after 50 h of operation. The thermal stability of Cu–Mn catalysts may be attributed to stabilization of metallic copper particles formed under reaction conditions due to interaction with the host oxide MnO [27,28].

4. Conclusion

Combustion-synthesized Cu–Mn spinel oxide catalysts are highly active for the production of H_2 via (combined) steam reforming of methanol despite their low surface area. Their activity is comparable to that of commercial Cu–Zn–Al catalysts. XRD analysis of fresh catalysts revealed that they are composed of the spinel phase $Cu_{1.5}Mn_{1.5}O_4$, as well as of Mn_2O_3 and CuO, depending on the Cu/Mn ratio. Exposure of the catalysts to the methanol-reforming reaction mixture resulted in the reduction/decomposition of the spinel oxide and formation of reduced species of copper and manganese. XPS analysis revealed the presence of two different oxidation states in both copper (Cu^{2+} and Cu^{+}) and manganese (Mn^{4+} and Mn^{3+}) in fresh catalysts and decomposition of the spinel in used catalysts. XRD and TPR measurements showed that at a high copper content ($x = 0.40$, 0.50), the excess copper was not incorporated into the spinel, but rather was present as a separate CuO phase. A transient reduction/oxidation behavior was seen in the course of successive TPR/TPO cycles, as the efficiency of spinel reformation during oxidation of the reduced catalyst gradually diminished. The optimal catalyst was prepared with a Cu/(Cu + Mn) ratio of 0.30, and the catalytic performance as a function of copper content was in agreement with the results of characterization analysis. A simple power-law rate expression with reaction orders of 0.7 (methanol) and 0.5 (water) provided a good fitting of the kinetic data. Product hydrogen, on the other hand, inhibited the reaction. The amount of CO produced during reforming process was well below that predicted by the WGS equilibrium, indicating that CO_2 was the product of steam reforming, whereas CO was produced by the reverse WGS reaction. TPO measurements performed after methanol-reforming runs indicated that carbon deposition was minimal.

Acknowledgment

The work was carried out in the framework of the EPAN E-25 project with funding from the General Secretariat for Research and Technology, Ministry of Development, Greece.

References

[1] J.J. Spivey, Catal. Today 100 (2005) 171.
[2] A. Basile, G.F. Tereschenko, N.V. Orekhova, M.M. Ermilova, F. Gallucci, A. Iulianelli, Int. J. Hydrogen Energy 31 (2006) 1615.
[3] J.-P. Shen, C. Song, Catal. Today 77 (2002) 89.
[4] S. Muscia-Mascarós, R.M. Navarro, L. Gómez-Sainero, U. Constantino, M. Ncchetti, L.G. Fierro, J. Catal. 198 (2001) 338.
[5] M. Lyubovsky, S. Roychoudhury, Appl. Catal. B Environ. 54 (2004) 203.
[6] S. Liu, K. Takahashi, K. Uematsu, M. Ayabe, Appl. Catal. A Gen. 283 (2005) 125.
[7] N. Iwasa, M. Yoshikawa, W. Nomura, M. Arai, Appl. Catal. A Gen. 292 (2005) 215.
[8] T.J. Huang, S.W. Wang, Appl. Catal. 24 (1983) 287.
[9] T.J. Huang, S.L. Chren, Appl. Catal. 40 (1988) 43.
[10] S. Velu, K. Suzuki, M. Okazaki, M.P. Kapoor, T. Osaki, F.J. Ohashi, J. Catal. 194 (2) (2000) 373.
[11] S. Velu, K. Suzuki, M.P. Kapoor, F. Ohashi, T. Osaki, Appl. Catal. A Gen. 213 (2001) 47.
[12] S. Velu, K. Suzuki, Top. Catal. 22 (2003) 235.

[13] J. Agrell, H. Birgersson, M. Boutonnet, I. Melián-Cabrera, R.M. Navarro, J.L.G. Fierro, J. Catal. 219 (2003) 389.
[14] T.L. Reitz, S. Ahmed, M. Krumpelt, R. Kumar, H.H. Kung, J. Mol. Catal. A 162 (2000) 275.
[15] J. Papavasiliou, G. Avgouropoulos, T. Ioannides, Catal. Commun. 5 (2004) 231.
[16] J. Papavasiliou, G. Avgouropoulos, T. Ioannides, Appl. Catal. B Environ. 69 (2007) 226.
[17] W. Shan, Z. Feng, Z. Li, J. Zhang, W. Shen, C. Li, J. Catal. 228 (2004) 206.
[18] J. Papavasiliou, G. Avgouropoulos, T. Ioannides, Catal. Commun. 6 (2005) 497.
[19] G. Avgouropoulos, T. Ioannides, Appl. Catal. A Gen. 244 (2003) 155.
[20] D. Briggs, M.P. Seah, Practical Surface Analysis by Auger and X-Ray Photoelectron Spectroscopy, Wiley, Chichester, 1983.
[21] Y. Tanaka, T. Takeguchi, R. Kikuchi, K. Eguchi, Appl. Catal. A Gen. 279 (2005) 59.
[22] F.C. Buciuman, F. Patcas, T. Hahn, Chem. Eng. Proc. 38 (1999) 563.
[23] M.R. Morales, B.P. Barbero, L.E. Cadús, Appl. Catal. B Environ. 67 (2006) 229.
[24] X. Li, J. Xu, L. Zhou, F. Wang, J. Gao, C. Chen, J. Ning, H. Ma, Catal. Lett. 110 (2006) 149.
[25] Y. Tanaka, T. Utaka, R. Kikuchi, K. Sasaki, K. Eguchi, Appl. Catal. A Gen. 242 (2003) 287.
[26] A.S. Reddy, C. Gopinath, S. Chilukuri, J. Catal. 243 (2006) 278.
[27] Y. Tanaka, R. Kikuchi, T. Takeguchi, K. Eguchi, Appl. Catal. B Environ. 57 (2004) 211.
[28] Y. Tanaka, T. Utaka, R. Kikuchi, T. Takeguchi, K. Sasaki, K. Eguchi, J. Catal. 215 (2003) 271.
[29] S. Paldey, S. Gedevanishvili, W. Zhang, F. Rasouli, Appl. Catal. B Environ. 56 (2004) 227.
[30] A.A. Marzaei, H.R. Shaterian, M. Habibi, G.J. Hutchings, S.H. Taylor, Appl. Catal. A Gen. 253 (2003) 499.
[31] M. Oku, K. Hirokawa, S. Ikeda, J. Electron Spectrosc. 7 (1975) 465.
[32] P.A. Wright, S. Natarajan, M. Thomas, P.L. Gai-Boyes, Chem. Mater. 4 (1992) 1053.
[33] J.F. Marco, J.R. Cancedo, H. Nguyen Cong, M. del Canto, J.L. Gautier, Solid State Ionics 177 (2006) 1381.
[34] D.A. Kukuznyak, S.W. Han, M.H. Lee, K.A. Omland, M.C. Gregg, E.A. Stern, F.S. Ohuchi, J. Vac. Sci. Technol. 19 (2001) 1923.
[35] P. Porta, G. Moretti, M. Musicanti, A. Nardella, Solid State Ionics 63–65 (1993) 257.
[36] G.C. Allen, S.J. Harris, J.A. Jutson, J.M. Dyke, Appl. Surf. Sci. 37 (1989) 111.
[37] G. Fierro, S. Morpurgo, M. Lo Jacono, M. Inversi, I. Pettiti, Appl. Catal. A Gen. 166 (1998) 407.
[38] F. Li, L. Zhang, D.G. Evans, X. Duan, Colloids Surf. A 244 (2004) 169.
[39] V.R. Galakhov, M.A. Korotin, N.A. Ovechkina, E.Z. Kurmaev, V.S. Gorshkov, D.G. Kellerman, S. Bartkowski, M. Neumann, Eur. Phys. J. B 14 (2005) 281.
[40] A. Wollner, F. Lange, H. Schmelz, H. Knozinger, Appl. Catal. A Gen. 94 (1993) 181.
[41] G. Jernigan, G.A. Somorjai, J. Catal. 147 (1994) 567.
[42] G.J. Hutchings, A.A. Mirzaei, R.W. Joyner, M.R.H. Siddiqui, S.H. Taylor, Appl. Catal. A Gen. 166 (1998) 143.
[43] J.K. Lee, J.B. Ko, D.H. Kim, Appl. Catal. A Gen. 278 (2004) 25.
[44] H. Purnama, T. Ressler, R.E. Jentoft, H. Soerijanto, R. Schogl, R. Schomacker, Appl. Catal. A Gen. 259 (2003) 83.
[45] J.C. Amphelett, M.J. Evans, R.F. Mann, R.D. Weir, Can. J. Chem. Eng. 63 (1985) 605.
[46] V. Agarwal, S. Patel, K.K. Pant, Appl. Catal. A Gen. 279 (2005) 155.
[47] C.J. Jiang, D.L. Trimm, M.S. Wainright, N.W. Cant, Appl. Catal. A Gen. 93 (1993) 245.
[48] J. Agrell, M. Boutonnet, J.L.G. Fierro, Appl. Catal. A Gen. 253 (2003) 213.
[49] J. Agrell, H. Birgersson, M. Boutonnet, J. Power Sources 106 (2002) 249.
[50] R.O. Idem, N.N. Bakhshi, Chem. Eng. Sci. 51 (1996) 3697.
[51] B. Lindstrom, L.J. Pettersson, P.G. Menon, Appl. Catal. A Gen. 234 (2002) 111.
[52] B. Frank, F.C. Jentoft, H. Soerijanto, J. Kröhnert, R. Schlögl, R. Schomäcker, J. Catal. 246 (2007) 177.